

# Numerical Simulations of Galaxy Formation

Matthias Steinmetz\*  
*Steward Observatory*  
*University of Arizona*  
*Tucson, AZ 85721, USA*

**Abstract.** The current status of numerical simulations of galaxy formation is reviewed. After a short description of the main numerical simulation techniques, three sample applications illustrate how numerical simulations have provided deeper insight in the galaxy formation process and how they have illuminated success and failure of the hierarchical galaxy formation paradigm: N-body simulations demonstrate that the density profiles of dark matter halos that form in hierarchical clustering scenarios follow a characteristic law. A comparison with the kinematics of disk galaxies however unravels that these density profiles are too concentrated. Hydrodynamical simulation show that the highly irregular velocity field of merging subclumps at redshift  $z \approx 3$  can easily account for the observed asymmetry in the absorption profiles of low ionization species in damped Ly- $\alpha$  absorption systems. The built-up of galaxies due to mergers is however also cause for one of the major inconsistencies of hierarchical structure formation models, the failure to reproduce the sizes of the present day disk galaxies due to excessive transport of angular momentum from the baryonic to the dark matter component. Hydrodynamical simulations that include star formation show that scaling laws like the Tully–Fisher relation can readily be reproduced in hierarchical scenarios, however the high concentration of dark matter halos results in a zero-point of the simulated Tully–Fisher relation that is incompatible with observations.

## 1. Introduction

The past couple of years have witnessed a dramatic increase in the quantity and quality of observations on the formation and evolution of galaxies. Galaxies are routinely identified at redshifts exceeding three and high resolution imaging allows us to study their internal structure. These data are complemented by high resolution spectroscopy of QSO absorption systems that provide further clues on the evolution of baryons in the universe. In fact this increase has been so rapid that observations have outgrown their theoretical framework. Traditional approaches, which rely heavily on the morphological classification of galaxies and which intend to disentangle the star formation history of galaxies, seem outdated if compared with the much richer structure seen in galaxies at different redshifts.

Motivated by the increasing body of evidence that most of the mass of the universe consist of invisible “dark” matter, and by the

---

\* Alfred P. Sloan Fellow, David and Lucile Packard Fellow



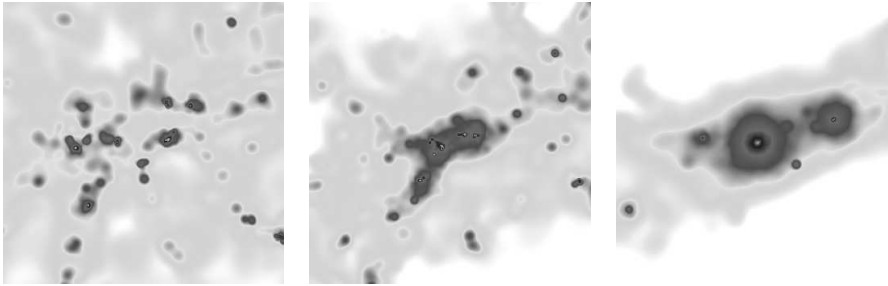


Figure 1. Hierarchical galaxy formation: Three plots showing the projected density of a forming galaxy at  $z = 4$  (left),  $z = 2$  (middle) and  $z = 0$  (right). The box has a side length of 2.8 Mpc (comoving).

particle physicist’s inference that this dark matter consists of exotic non-baryonic particles, a new and on the long run much more fruitful approach has been developed: rather than to model the formation and evolution of galaxies from properties of present day galaxies, it is attempted to prescribe a set of reasonable initial conditions. The evolution of galaxies is then modeled based on physical processes that are considered to be relevant such as gravity, hydrodynamics, radiative cooling and star formation. The outcome at different epochs is then confronted against observational data.

One scenario that has been extensively tested in that way is the model of hierarchical clustering, currently the most successful paradigm of structure formation. The initial conditions consist of the cosmological parameters ( $\Omega$ ,  $\Lambda$ ,  $H_0$ ) and of an initial fluctuation spectrum such as the *cold dark matter* (CDM) spectrum. The remaining free parameter, the amplitude of these initial fluctuations, is calibrated by observational data, e.g., the measured anisotropies of the microwave background. Structure then grows as systems of progressively larger mass merge and collapse to form newly virialized systems. This process is illustrated in figure 1, which shows the hierarchical build-up of a typical galaxy such as the Milky Way.

These *ab-initio* models can be split in two major categories: (i) Semianalytical (or phenomenological) models (henceforth SAMs) describe the physical processes that affect the formation of galaxies by simple, physically motivated recipes (Kauffmann, Guiderdoni & White 1994; Cole et al. 1994). Free parameters are calibrated by comparison with a subset of observational data, e.g. the galaxy luminosity function. (ii) Numerical simulations model the dynamics and the interplay of these processes in detail. The boundary between these two categories is not very well defined. For example, hybrid models are commonly used in which the large-scale dynamics of the dark matter is modeled

by simulation while SAMs are employed in order to populate dark matter halos with galaxies (Kauffmann, Nusser & Steinmetz 1997). Also some commonly used star formation and feedback prescriptions in hydrodynamical galaxy formation models are not unlike the recipes used in SAMs (e.g. Navarro & White 1993).

SAMs have proven to be an extremely helpful tool to understand statistical properties of the galaxy population and how these properties change with redshift. Due to construction they miss, however, the capability to make strong predictions on the substructure and detailed morphology of galaxies. It is also at these galactic length scales (a few kpc) at which the assumptions that enter semianalytical models and the results of numerical simulations differ the most. For example, SAMs assume that while galactic halos collapse, gas is heated up to the virial temperature of the dark matter halo. Simulations however show that most of the gas is never heated to temperatures exceeding a few  $10^4$  K. SAMs also assume that the collapse of cooling gas into a rotationally supported disk proceeds under conservation of angular momentum. Angular momentum transport between gas and dark matter is neglected, quite in contrast to the results of numerical simulations. I will come back to this issue in section 4.

This review intends to report on the state of the art of current computer simulation and to summarize what major results could be achieved. I start this review with an overview of the commonly used simulation techniques. I will then discuss in detail three examples that illuminate challenge, success and failure of numerical simulations of galaxy formation. Such a selection can only give a glimpse of the large body of results obtained in more than a thousand refereed publications over the last years addressing topics such as mass determination of X-ray clusters (Evrard, Metzler & Navarro 1996), gravitational lensing by galaxy clusters (Bartelmann & Steinmetz 1996), the physical properties of the Ly- $\alpha$  forest (Cen et al. 1994; Hernquist et al. 1996), the formation of first structures in the universe (Abel et al. 1998), or the reionization of the universe (Gnedin & Ostriker 1997), to name only a few.

## 2. Techniques

Over the past three decades quite a variety of numerical simulation techniques have been developed to simulate the formation of galaxies. These can be roughly classified into three subgroups: (i) collisionless simulations; (ii) hydrodynamical simulations; (iii) hydrodynamical simulations that include the effects of star formation.

## 2.1. COLLISIONLESS SYSTEMS

The distribution function  $f(\mathbf{r}, \mathbf{v}, t)$  of a system consisting of particles of mass  $m$ , which only interact by gravity, can mathematically be described by the Vlasov equation (collisionless Boltzmann equation):

$$\frac{df(\mathbf{x}, \mathbf{v}, t)}{dt} = \frac{\partial f}{\partial t} + \mathbf{v} \cdot \nabla f - \nabla \Phi \frac{\partial f}{\partial \mathbf{v}} = 0 \quad (1)$$

The gravitational potential is given by Poisson's equation

$$\Delta \Phi = 4\pi G \int d^3v m f(\mathbf{x}, \mathbf{v}, t). \quad (2)$$

An astrophysically relevant application of the Vlasov–Poisson system is the study of systems that only consists of stars and/or (weakly interacting) dark matter. It turns out, that  $N$ –body simulations provide a robust and efficient, although sometimes computationally expensive tool to numerically solve those equations.

In  $N$ –body–simulations, the trajectories of particles are determined by the laws of Newtonian dynamics

$$\frac{d\mathbf{v}_i}{dt} = -\nabla \Phi|_i \quad (3)$$

$$\Phi(\mathbf{r}_i) = -G \sum \frac{m_j}{|\mathbf{r}_j - \mathbf{r}_i|}. \quad (4)$$

Every particle of a  $N$ –body–simulation represents a huge number of dark matter particles (compare the mass of a body in the simulation (typically  $10^8 - 10^{12} M_\odot$ ) with that of an elementary particle (100 GeV)!).  $N$ –body–simulations can, therefore, be interpreted as a Monte–Carlo–Approximation of the Vlasov equation, i.e. the set  $(\mathbf{r}_i(t), \mathbf{v}_i(t), i = 1, N)$  samples the distribution function  $f(\mathbf{r}, \mathbf{v}, t)$ . This is a major conceptual difference to  $N$ -body simulations used to model planetary systems or star clusters in which each particle intends to mimic an actual physical body !

## 2.2. HYDRODYNAMICAL SIMULATIONS

If collisions between particles (e.g. ions) can no longer be neglected, Vlasov's equation must be replaced by Boltzmann's equation  $\frac{df}{dt} = [\frac{df}{dt}]_c$ , the latter term describing the change in the distribution function due to collisions. However, if the mean free path of a particle is small compared to the typical scale of the object under consideration and if the force between particles is short ranged, a moment expansion of Boltzmann's

equation results in the well know hydrodynamical conservation laws. In so-called Lagrangean coordinates, i.e. coordinates that co-move with a fluid element, these equations read:

$$\frac{d\rho}{dt} = -\rho\nabla\mathbf{v} \quad (5)$$

$$\frac{d\mathbf{v}}{dt} = -\frac{1}{\rho}\nabla P - \nabla\Phi \quad (6)$$

$$\frac{d\varepsilon}{dt} = -\frac{P}{\rho}\nabla\mathbf{v} + \frac{Q - \Lambda(\rho, T)}{\rho}, \quad (7)$$

where  $\rho$  is the density of the fluid,  $\mathbf{v}$  its velocity,  $P$  its pressure and  $\varepsilon$  the specific thermal energy, respectively.  $\Phi$  is the gravitational potential. Equation (6) is usually referred to as ‘‘Euler’s equation’’. The energy equation (7) is derived from the first law of thermodynamics.  $\Lambda$  and  $Q$  denote energy sinks and sources. The system is closed by Poisson’s equation (2) and by an equation of state, which in the case of an ideal gas reads

$$P = (\gamma - 1)\varepsilon\rho \quad (8)$$

with  $\gamma = \frac{5}{3}$ .

### 2.3. HYDRODYNAMICAL SIMULATIONS INCLUDING STAR FORMATION

While collisionless and hydrodynamical simulations differ on a very elementary level, such a distinction cannot be made between simulations that neglect/include star formation. The only difference at an elementary level is that in simulations that include the effects of star formation matter, momentum and energy is exchanged between the collisional (gas) and a collisionless (stars) component by processes other than gravity. The distinction between simulation with and without star formation thus appears to be somewhat arbitrary. I nevertheless consider this discrimination to be valid as a new element enters: phenomenological modeling. While so far equations were governed by basic statistical and/or atomic physics, the effects of star formation cannot be reduced to such a fundamental level. Actually our understanding of the star formation process and its interaction with the surrounding interstellar medium is rather limited. The best that we can do (at least on the macroscopic scale of a galaxy) is to empirically parameterize the problem. Most models so far follow an implementation similar to that outlined by Katz (1992): It is assumed that the star formation rate  $\frac{d\rho_*}{dt}$  is proportional to the local gas density divided by the local dynamical time scale

$$\frac{d\rho_*}{dt} = c_* \frac{\rho_{\text{gas}}}{\tau} \quad (9)$$

$c_*$  being the star formation efficiency, typically a factor of a few per cent. Since the local dynamical time scale  $\tau$  is proportional to  $1/\sqrt{G\rho}$ , the star formation rate grows with the gas density like  $\rho^{1.5}$ . Over a typical star formation time step  $\Delta t$ , a collisionless star particle (which represents of the order of a few million stars) of mass

$$m_* = m_{\text{gas}} \left( 1 - \exp \left( -\frac{c_* \Delta t}{\tau} \right) \right) \quad (10)$$

is created and the mass of the gas particle/mesh cell is correspondingly reduced. Over the lifetime of a high mass star the supernovae energy is released and the corresponding mass and energy injected to the gas. In Steinmetz & Müller (1994, 1995) supernovae also metal enrich the ISM. Simulations exhibit, however, that the energy injected by supernovae affects the dynamics of a galaxy only little. Since supernovae energy is added to gas in the neighborhood of a star forming region, local gas densities are very high and gas can cool very efficiently (see, however, Yepes et al. 1997). Indeed, Steinmetz & Müller (1995) have shown that the net energy loss, i.e. the difference between the energy injected by supernovae and the energy radiated away due to cooling, is almost identical in simulations with and without supernova feedback. Navarro & White (1993) however demonstrated that if energy is added to the kinetic energy, the effect of feedback can be quite drastic. Even in the case of a low feedback efficiency of about 1%, the energy released by the first supernovae is able to strongly suppress further star formation in galaxies with virial velocities less than about 100 km/sec.

#### 2.4. NUMERICAL SOLUTION

The numerical task that has to be performed is to solve a system of partial differential equations (PDEs), partially of elliptic (e.g. Poisson's equation) partially of hyperbolic (e.g. hydrodynamical equations) character. In order to solve these PDEs, quite a number of techniques have been developed that roughly can be split in two groups:

- Mesh based methods discretize the PDEs on a mesh and solve the corresponding difference equation. Most hydrodynamical schemes are mesh based.
- Particle based methods reformulate (e.g. by using kernel estimates) the PDEs into a set of equations of motion coupled by inter-particle forces. The so-called *smoothed particle hydrodynamics* (SPH) scheme, the most widely used hydrodynamical method in extragalactic astronomy, is such a particle based method.

Both approaches have their disadvantages and their merits and the optimal choice is problem dependent. As a rule of thumb one can say that mesh based methods are faster and periodic boundary conditions, which are usually applied for cosmological simulations, are automatically implemented. Mesh based methods have also been shown to be superior in capturing shocks and in dealing with turbulence compared to SPH codes, which rely on artificial viscosity. The disadvantage is that the dynamical range is rather limited. Particle methods are computationally more expensive but have a much larger dynamic range. Furthermore, periodic boundaries are not automatically provided but have to be added explicitly, e.g. by means of the Ewald summation technique (Ewald 1921; Hernquist, Bouchet & Suto 1991). More recently, adaptive mesh refinement (AMR) techniques (e.g. Abel et al. 1998; Kravtsov et al. 1998) have been developed that combine the merits of particle and mesh based methods, however at the expense of a very high code complexity. Almost all techniques have been adapted to run well on vector- and massively parallel computers. Particle methods can also run quite efficiently on a workstation using GRAPE (Sugimoto et al. 1990; Steinmetz 1996), a chip especially designed to solve the gravitational N-body problem.

### 3. N-body simulations – Density profiles of dark matter halos

N-body simulation are still the most widely used simulation technique to study the formation of objects on the largest scales. Most simulations performed in the seventies and eighties, however, suffered from an insufficient dynamic range. Those simulations were unable to cover a statistically representative volume and to simultaneously resolve individual dark matter halos. Consequently, cosmological simulation mainly concentrated on the statistical distribution of matter (e.g. determine the two-point correlation function). In the best case, global properties of dark matter halos such as mass and angular momentum could be determined (Barnes & Efstathiou 1987). Simulations that focussed on the formation of individual galaxies (e.g. van Albada 1982; Barnes & Hernquist 1992) were performed decoupled from a cosmological context.

In recent years, the increasing computer power and the advent of new simulation techniques allowed to study the formation of an individual object in its full cosmological context. Multi-mass/AMR simulation techniques (Navarro & Benz 1991; Katz & White 1993; Bartelmann, Steinmetz & Weiss 1995) resolve individual dark matter halos with several ten thousand particles (Navarro, Frenk & White 1996, 1997), or,

more recently, even several million particles (Moore et al. 1998; Klypin et al. 1998).

These advanced simulations addressed one of the key problems in cosmology, the profile of dark matter halos and thus the shape of the rotation curves of galaxies, one of the major observations that lead to the postulation of the dark matter dominated universe (e.g. Rubin, Thonnard & Ford 1978). Navarro, Frenk & White (1996, 1997, henceforth NFW) found that the density profiles of halos follow a universal law, which can be parameterized by

$$\frac{\varrho(r)}{\varrho_b} = \frac{\delta_n}{\frac{r}{r_s}(1 + \frac{r}{r_s})^2}. \quad (11)$$

The two parameters are the scale radius  $r_s$ , which defines the scale where the profile shape changes from slope  $\alpha > -2$  to  $\alpha < -2$ , and the characteristic overdensity  $\delta_n$ . They are related because the mean overdensity enclosed within the virial radius  $r_{\text{vir}}$  is 200. The slope of the profile  $\alpha = d \ln \varrho / d \ln r$  approaches  $\alpha = -1$  near the halo center and  $\alpha = -3$  at large radii. At intermediate radii (typically several tens of kpc),  $\alpha \approx -2$  resulting in a flat rotation curve. Equation (11) differs slightly in its asymptotic behavior at large radii from the profile that was proposed by Hernquist (1990) to describe the mass profiles of elliptical galaxies. This profile, which goes like  $r^{-4}$  at large radii, was used by Dubinsky & Carlberg (1991) to fit the density distribution of halos that were formed in their CDM-like simulation.

Cole & Lacey (1996), Tormen, Bouchet & White (1997), Moore et al. (1998) and Huss, Jain & Steinmetz (1999a), among others, have extended the original results of NFW to other initial spectra, to other cosmologies and to higher spatial and mass resolution. Most of the above studies show that halos that form in a variety of cosmological models are well described by equation (11). These results suggest that the density profile found by NFW is quite generic for any scenario in which structures form due to hierarchical clustering, although the slope of the density at small radii is still matter of some debate (see, e.g., Moore et al. 1998 and Kravtsov et al. 1998). The power spectrum and cosmological parameters only enter by determining the typical formation epoch of a halo of a given mass and thereby the dependence of the characteristic radius  $r_s$  on the total mass of the halo. For *cold dark matter* type simulations that are normalized to abundance of massive galaxy clusters, the concentration parameter  $c = r_{\text{vir}}/r_s$  seems to depend only very little on the actual cosmological parameters  $\Omega$  and  $\Lambda$ . The initial value given by NFW was  $c \approx 10 - 15$  while recent higher resolved simulations find this value to be about 40% higher,  $c \approx 15 - 20$  (Moore et al. 1999a; Navarro & Steinmetz 1999).



The actual physical mechanisms responsible for such an universal density profile are as of yet not well understood. Syer & White (1997) argued that the key to the NFW profile lies in the hierarchical merging history of cold dark matter halos. Huss, Jain & Steinmetz (1999b) however found that even in hot dark matter simulations and also in 3D spherically collapse simulations the profiles of dark matter halos are well fit by a NFW profile. Similar results have also been obtained by Moore et al. (1999a) for a warm dark matter model. Huss et al. (1999b) argue that the universal profile is a more generic feature of gravitational collapse in a cosmological setting and is related to the angular momentum distribution of halos. The mechanism by which angular momentum is acquired can vary, potential mechanism include merging (for hierarchical models) and radial orbit instabilities (for spherical collapse models).

The existence of such an universal density profile makes strong predictions on the shape of the rotation curve of galaxies that can be confronted against observations. Such a test on galactic scales is particularly interesting since few observational constraints on such small scales have been used to adjust the parameters of the different flavors of the cold dark matter scenario. Such a comparison reveals that the asymptotic slope of the density profile at small radius of  $\alpha = -1$ , seems at odds with rotation curve studies of dark matter-dominated galaxies (Moore 1994; Flores & Primack 1994; McGaugh & De Block 1998; Moore et al. 1999a; Navarro 1999). Unfortunately, the scales where deviations are most pronounced (the inner few kpc) are also the most compromised by numerical uncertainties (most simulations relevant to this problem published to date have gravitational softening scales of order 1 kpc). The comparison is thus rather uncertain. For example, Kravtsov et al. (1998) have argued, on the basis of simulations similar to those used by the other authors, that CDM halos are actually *consistent* with the rotation curves of dark matter-dominated disks, a somewhat surprising result that illustrates well, nonetheless, the vulnerability of numerical techniques on scales close to the numerical resolution of the simulations.

In order to circumvent these problems, Navarro & Steinmetz (1999, henceforth NS99) used, rather than the dark matter density profile near the center, the *total amount* of dark mass within the main body of individual galaxies. For spiral galaxies, this criterion implies that simulations that can estimate reliably the amount of dark mass within a couple of exponential scalelengths may be safely used for comparison with observations. For bright spirals like the Milky Way this corresponds to radii of about 5-10 kpc, well outside the region that may

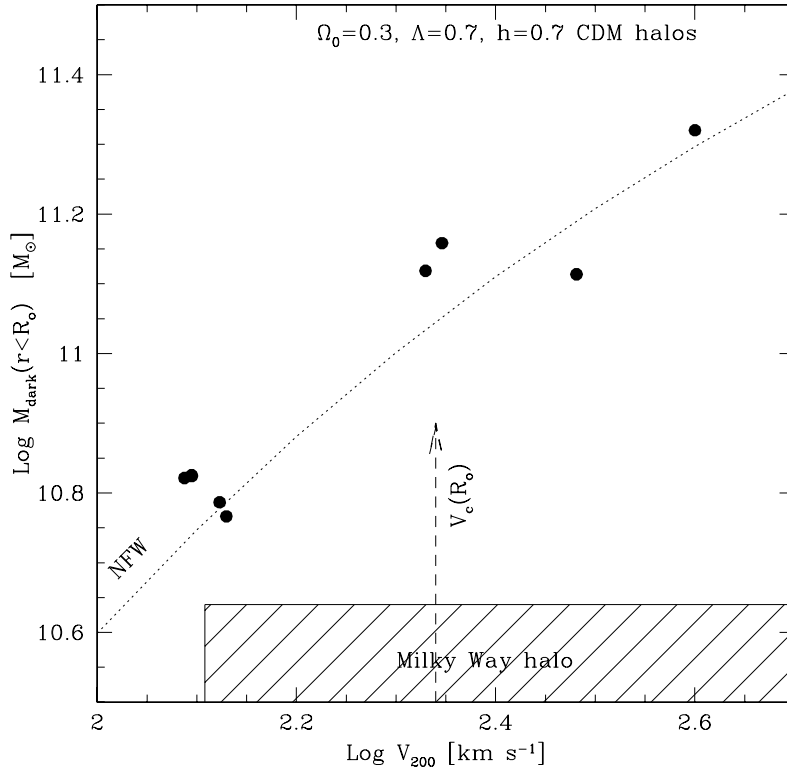


Figure 2. Dark mass enclosed within a radius  $R_o = 8.5$  kpc, the Sun’s distance from the center of the Milky Way, versus the circular velocities of  $\Lambda$ CDM halos. The shaded region highlights the allowed parameters of the dark halo surrounding the Milky Way, as derived from observations of Galactic dynamics and by assuming that the disk mass cannot exceed the total baryonic content of the halo. The filled circles show the loci of  $\Lambda$ CDM halos as determined from high-resolution N-body simulations. The solid line is the circular velocity dependence of the dark mass expected inside  $R_o$  for halos that follow the density profile proposed by NFW. The circular velocity dependence of the NFW “concentration” parameter of the simulated halos is well approximated on these scales by  $c \approx 20 (v_{\text{vir}}/100 \text{ km s}^{-1})^{-1/3}$  (dotted line).

be compromised by numerical artifacts in the current generation of N-body experiments.

The argument to constrain the total amount of dark matter within the solar circle  $R_0$  goes as follows:

- The total stellar mass of the Milky Way puts a lower limit on the total baryonic mass enclosed within the virial radius of the Milky Way’s dark matter halo. Since the baryon to dark matter

ratio within the virial radius is the same as the cosmologically representative value (White et al. 1993), this puts a lower limit  $v_{\text{vir},\text{min}}$  on the mass and thus on the circular velocity of the Milky Way’s halo. Using N-body simulations, a lower limit  $M_{\text{DM},\text{lim}}$  on the mass within the solar circle can be deduced.

- The rotation velocity of the Milky Way can be translated into a total mass enclosed within the solar circle. By subtracting the observed stellar mass an upper limit on the observationally inferred mass within the solar circle  $M_{\text{DM},\text{est}}$  can be given.
- In order to be consistent with the observations,  $M_{\text{DM},\text{lim}}$  must be smaller than the  $M_{\text{DM},\text{est}}$  at least for some halos with  $v_{\text{vir}} > v_{\text{vir},\text{min}}$ .

The main difficulty in this argument is a proper estimate of potential observational uncertainties. This analysis has been done in NS99, the results are shown in figure 2, which compares, as a function of halo mass, the dark mass estimate  $M_{\text{DM},\text{est}}$  with the results of simulations of several  $\Lambda$ CDM halos. Halo masses ( $M_{\text{vir}}$ ) are measured inside the radius,  $r_{\text{vir}}$ , of a sphere of mean density 200 times the critical density for closure, and are typically characterized by the circular velocity at that radius. The comparison shows clearly a major discrepancy between the maximum dark matter inside  $R_o$  allowed by observations and the results of the numerical experiments. For example,  $\Lambda$ CDM halos with circular velocities similar to that of the Milky Way disk ( $v_{\text{vir}} \approx v_{\text{rot}}(R_o) = 220 \text{ km s}^{-1}$ ) have about *three times* more dark mass inside the solar circle than inferred from observations. Even for the extreme case where the halo has the strict minimum circular velocity  $v_{\text{vir},\text{min}}$ , the simulations indicate an excess of more than 50% in the dark mass within  $R_o$ .

This serious discrepancy only worsens if some extra dark material is drawn inside  $R_o$  by the formation of the disk. A rough estimate of the magnitude of this correction can be made by assuming that the halo responds adiabatically to the assembly of the disk; the discrepancy then increases from 50% to almost 80% for the least massive halo. Halos formed in the  $\Lambda$ CDM scenario are too centrally concentrated to be consistent with observations of the dynamics of the Galaxy.

The results thus confirm the problem already seen in the rotation curves of disk galaxies, that dark matter halos as they form in a cold dark matter scenario are too concentrated. A related problem has been recently published by Moore et al. (1999a,b) and by Klypin et al. (1999) who demonstrate that cold dark matter scenarios predict that the local group should host fifty times as many dwarf galaxies than actually observed. In order to reconcile the cold dark matter scenario, a power

spectrum would be required that suppresses power on galactic and subgalactic scales while keeping the large scale properties of the model virtually unchanged. This would in principle allow galaxy-sized dark halos to collapse later and thus become less centrally concentrated. One problem that afflicts such a modification is that they may hinder the formation of massive galaxies at high redshift, at odds with the mounting evidence that such galaxies are fairly common at  $z \gtrsim 3$  (see, e.g., Steidel et al. 1998).

#### 4. Hydrodynamical simulations – The kinematics of damped Ly- $\alpha$ systems

The major advantage of hydrodynamical simulations compared to N-body simulations is that they model the dynamics of the *visible* matter. Although hydrodynamical simulations were considerably successful in understanding the details of the galaxy formation process, the largest impact so far is related to the properties of QSO absorption systems where numerical simulations can explain the basic properties of QSO absorbers covering many orders of magnitude in column density (Cen et al. 1994; Hernquist et al. 1996; Zhang, Anninos & Norman 1995). Indeed, hydrodynamical simulation were responsible for a paradigm shift as QSO absorbers are no longer considered to be caused by individual gas clouds. Absorbers of different column density (Ly- $\alpha$  forest, metal line systems, Lyman limit systems and damped Ly- $\alpha$  absorption systems) are rather reflecting different aspects of the large scale structure of the universe. While the lowest column density systems ( $\log N \approx 12-14$ ) arises from gas in voids and sheets of the “cosmic web”, systems of higher column density are produced by filaments ( $\log N \approx 14-17$ ) or even by gas that has cooled and collapsed in virialized halos ( $\log N > 17$ ).

The kinematics of damped Ly- $\alpha$  absorption systems (DLAS) at high redshift serves as a very nice example to demonstrate how oversimplifying assumption may lead to wrong implications on the validity of a cosmological model and to show how the full numerical treatment can avoid those artificial contradictions. DLASs have often been interpreted as large, high-redshift progenitors of present-day spirals that have evolved little apart from forming stars (Wolfe 1988). Kauffmann (1996), however, studied the evolution of DLASs in the CDM structure formation scenario in which disks form by continuous cooling and accretion of gas within a merging hierarchy of dark matter halos and found that the total cross section was dominated by disks with comparably low rotation velocities (typically 70 km/sec). Prochaska & Wolfe (1998)

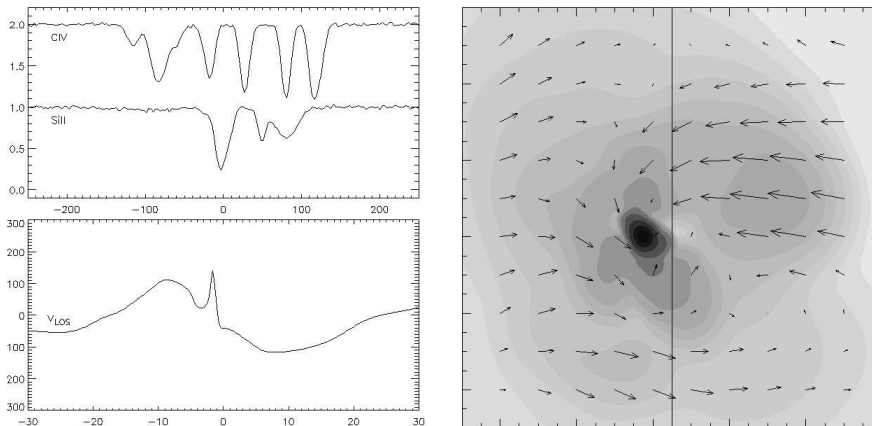


*Figure 3.* Right: Color map of the column density distribution in a 60 kpc around a damped system. Black correspond to HI densities  $\log n(HI) > 1.5$ , light grey to  $\log n(HI) \approx -3$ . White arrows indicate the velocity field. The white line correspond to the line-of-sight(LOS). In the lower left plot, the velocity field along the LOS is shown. The upper left plot shows the absorption line in CIV 1548 (top) and SiII 1808 (bottom). For readability, CIV has been displaced by 0.5 in flux.

however, observed much larger velocity spreads (up to 200 km/s) and came to the conclusion that only models in which the lines-of-sight (LOS) intersects rapidly rotating large galactic disks can explain both the large velocity spreads and the characteristic asymmetries of the observed low ionization species (e.g. , SiII) absorption profiles, in strong contradiction to the prediction of the (semianalytical) cold dark matter model.

So how may a numerical simulation solve this problem ? The critical assumption that enters the semianalytical models is that DLASs are equilibrium disks. Numerical simulations (Haehnelt, Steinmetz & Rauch 1998) show, however, that this is a poor assumption and that asymmetries and non-equilibrium effects play an important role. Figure 3 shows a typical configuration that gives rise to a high redshift DLAS with an asymmetric SiII absorption profile. The velocity width of about 120 km/s is also quite similar to typical observations. However, no large disk has yet been developed and also the circular velocity of the collapsed object is only 70 km/s. The physical structures that underly DLASs are turbulent gas flows and inhomogeneous density structures related to the merging of two or more clumps, rather than large rotating disks similar to the Milky Way. Rotational motions of the gas play only a minor role for these absorption profiles. A more detailed analysis also demonstrates that the numerical models easily pass the statistical

tests proposed by Prochaska and Wolfe, i.e., hierarchical clustering, in particular the CDM model, is consistent with the kinematics of high- $z$  DLASs.

While the irregular structure of a galaxy in the process of formation was helpful to alleviate the problem concerning the kinematics of DLASs, one may wonder whether it hurts the assembly of large galactic disks at low redshifts as major mergers are usually associated with the transformation of spirals into ellipticals (for a review, see Barnes & Hernquist 1992). Figure 4 indicates that on a qualitative level this seems not to be a problem. Although the gas is accreted in a fairly lumpy manner, at redshift  $z = 0$  a nice disk like structure has developed.

However, a closer look at the detailed structure reveals a major shortcoming of these disks, they are too concentrated (Navarro & Benz 1991; Navarro, Frenk & White 1995; Navarro & Steinmetz 1997). This, however, is not a problem in semianalytical models, which relatively easily can reproduce the sizes of present day galaxies. One may again ask: What is the difference between the semianalytical model (Mo, Mao & White 1997) and the numerical simulations, in particular since they are based on the same structure formation model? And again the reason can be found in the assumptions that enter the semianalytical models: Semianalytical models assume that gas collapses under conservation of angular momentum (Fall & Efstathiou 1980), an assumption that, as will be shown, is only very poorly fulfilled.

Figure 5 (left) shows the specific angular momentum of dark matter halos and of their central gaseous disks at  $z = 0$ , as a function of mass. If, as suggested by Fall & Efstathiou (1980), the collapse of gas would proceed under conservation of angular momentum, the baryonic component would have the same specific angular momentum  $J/M$  as the dark matter, however, its corresponding mass would be a factor of 20 smaller (for  $\Omega_{\text{bary}} = 0.05$ ,  $\Omega_0 = 1$ ). These disks would be located only slightly below the box for spiral galaxies. However, figure 5 demonstrates clearly that the spins of gaseous disks are about an order of magnitude lower than that. This is a direct consequence of the formation process of the disks. Most of the disk mass is assembled through mergers between systems whose own gas component had previously collapsed to form centrally concentrated disks. During these mergers, and because of the spatial segregation between gas and dark matter, the gas component transfers most of their orbital angular momentum to the surrounding halos. While the specific angular momentum of dark matter halos increases with decreasing redshift, that of gaseous disk decreases (figure 5 (right)).

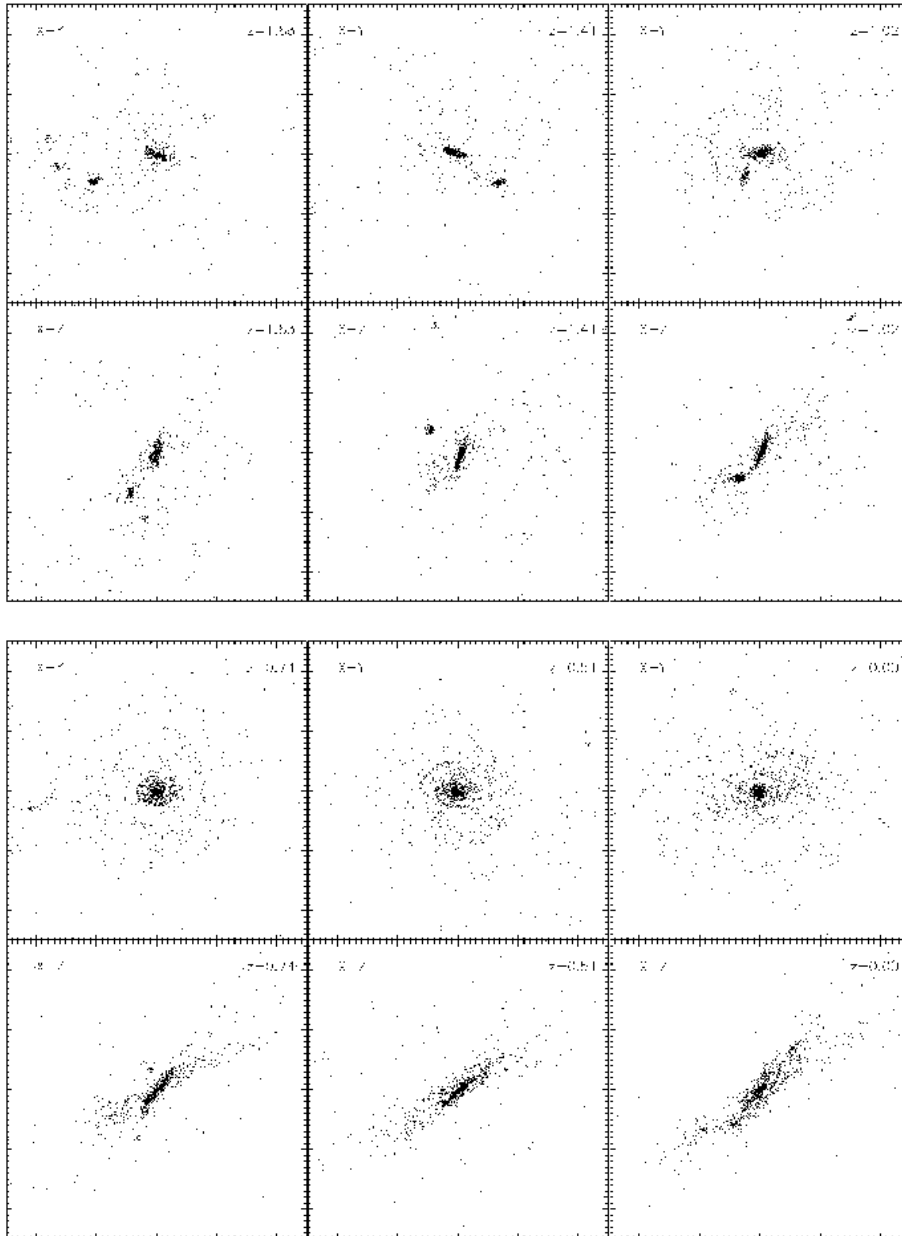


*Figure 4.* The distribution of gas projected in the X-Y and Y-Z plane shown for 6 different redshifts. The gas infall is mainly lumpy. Diffusely infalling gas settles to form a rotationally supported disk.

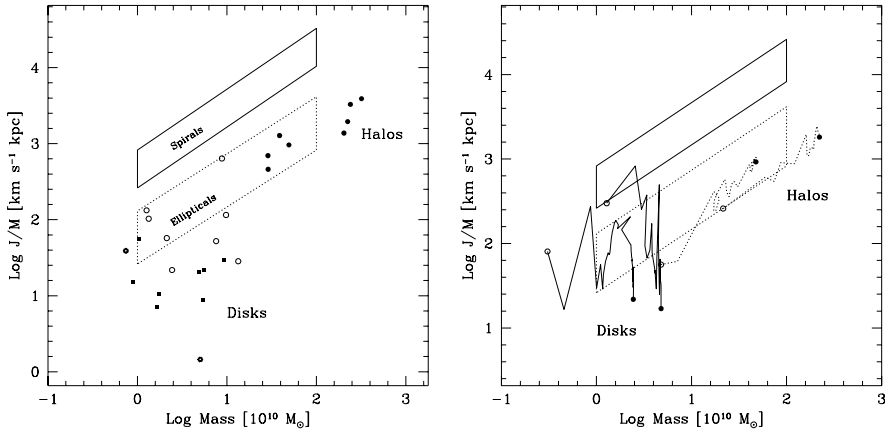


*Figure 5.* The specific angular momentum of dark halos and gaseous disks, as a function of mass. The boxes enclose the region occupied by spiral and elliptical galaxies, as given by Fall (1983). Open circles, solid squares and starred symbols correspond to the specific angular momenta of gaseous disks, solid circles for the hosting dark matter halos. Right: Evolution of the dark halo and central gaseous disk in the  $J/M$  versus  $M$  plane, from  $z = 5$  (open circles) to  $z = 0$  (solid circles). The mass of the system grows steadily by mergers, which are accompanied by an increase in the spin of the halo and a decrease in the spin of the central disk. The latter results from angular momentum being transferred from the gas to the halo during mergers.

## 5. Hydrodynamical simulations including star formation – The Tully Fisher relation

Some of the problems mentioned in the former sections may be alleviated by including star formation and related feedback processes such as stellar winds and supernovae (see e.g. Weil, Eke & Efstathiou, 1998). The major stumbling block designing such a simulations is the choice of a reasonable star formation recipe and the calibration of free parameters. The simulations presented in this section were performed using the star formation recipe as described in section 2.3. The star formation efficiency was calibrated such that a Kennicutt type relation between gas surface density and star formation can be reproduced (Kennicutt 1998).

Figure 6 illustrates the formation history of such a galaxy: The star formation rate peaks at early times (lookback time  $\approx 11$  Gyr) due to the nearly simultaneous collapse of a number of halos that later on merge to form two spiral galaxies. The star formation rate in each progenitor rarely exceeds  $\sim 1 M_{\odot}/\text{yr}$ , although its combined rate can reach about  $8 M_{\odot}/\text{yr}$ . The star formation rate in the two galaxies, which have formed by  $t_{\text{lookback}} = 7$  Gyr, is fairly constant and slowly declining. The two



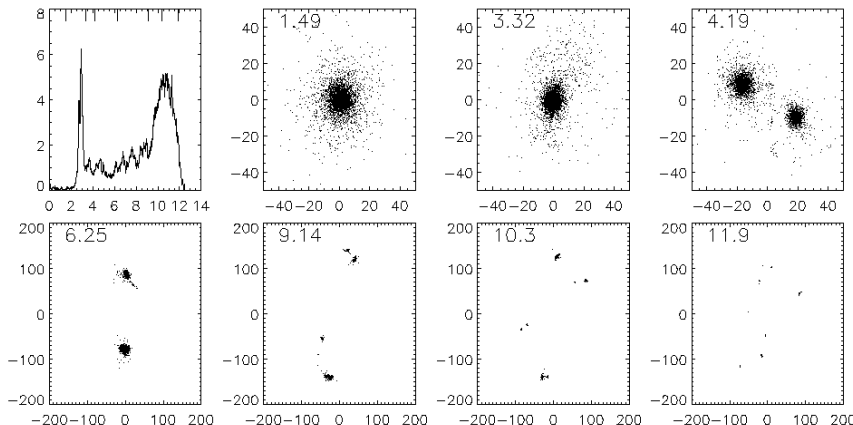


Figure 6. Upper left: Star formation rate (in  $M_{\odot}/\text{yr}$ ) versus lookback time of a forming galaxies (circular velocity  $\approx 100$  km/sec. Other plots: seven snapshots of the star particle distribution of the forming galaxy. Lookback time for each snapshot is given in the upper left corner.

galaxies merge at  $t_{\text{lookback}} = 3$  Gyr. Due to the merger gas streams to the center in a fashion similar to that described in Mihos & Hernquist (1994) where it is rapidly transformed into stars. The resulting “star burst” consumes almost all the gas and star formation at  $t_{\text{lookback}} < 2$  Gyr is essentially quenched, resulting in the formation of an elliptical galaxy. Galaxies that do not experience such a major merger at later epoch (not shown) continue to slowly transform gas into stars.

The success of such a model can be further assessed by testing, to what extent such a model can reproduce scaling relations that link total luminosity, rotation speed, and angular momentum of disk galaxies such as the Tully–Fisher (TF) relation. Figure 7 shows the results of such an investigation, the simulated  $I$ -band TF relation at  $z = 0$  for two cosmological scenarios, a standard CDM ( $\Omega = 1, \Lambda = 0$ ) and a  $\Lambda$ CDM ( $\Omega = 0.3, \Lambda = 0.7$ ) scenario. The simulated TF relation is compared with the data of Giovanelli et al. (1997), Mathewson, Ford & Buchhorn (1992) and Han & Mould (1992). The slope and scatter of the simulated TF relation are in fairly good agreement with the observational data. This results also holds in other bandpasses: the model TF relation becomes shallower (and the scatter increases) towards the blue, just as in observational samples (see Steinmetz & Navarro 1999). The model TF relations are also very tight. In the  $I$ -band the rms scatter is only 0.25 mag, even smaller than the observed scatter of  $\sim 0.4$  mag. This must be so if the results are to agree with observations: scatter in the models reflects the intrinsic dispersion in the TF relation, whereas the observed scatter includes contributions from both observational

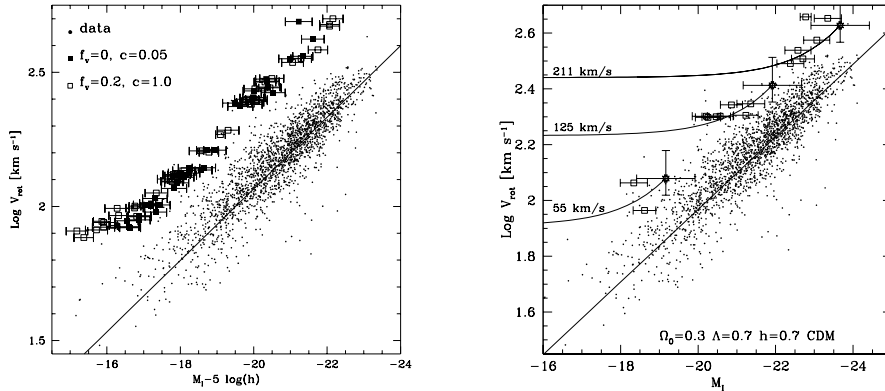


Figure 7. Left: I-band TF relation at  $z = 0$  for an  $\Omega = 1, \Lambda = 0$  CDM scenario. The error bars in the simulated data span the difference in magnitudes that results from adopting a Salpeter or a Scalo IMF. Right: I-band TF relation at  $z = 0$  for  $\Omega_b = 0.3, \Lambda = 0.7, h = 0.7$  CDM. See text for details.

errors and intrinsic dispersion. If, as it is usually argued, both effects contribute about equally to the observed dispersion in the TF relation, then the intrinsic scatter in the I-band should be comparable to the  $\sim 0.25$  mag found in the models.

The zero-point is, however, in serious disagreement with the data, the simulated TF relation being almost two magnitudes too faint at given rotation speed. One may argue that the discrepancy is related to the particular star formation and feedback parameterization, however very similar results can be obtained for quite different star formation prescriptions (Navarro & Steinmetz, in preparation).

In order to further understand the physical origin of the success and failure of the TF modelling, I will focus on the following three questions: (i) Why is the slope in such good agreement? (ii) Why is the scatter so small, in particular considering that the variation in the star to dark matter ratio changes quite substantially between individual halos? (iii) What causes the offset in the zero-point of the TF relation?

The first question is rather straight forward to answer (see e.g. Mo, Mao & White 1998): The slope is just a moderate modulation of the  $M \propto v^3$  scaling of dark matter halos that reflects the approximately scalefree process of assembly of collisionless dark matter into collapsed, virialized systems.

So why is the scatter so small although the star to gas ratio between individual halos varies by a factor of three to five? The answer is related to the dependence of the rotation velocity of the galactic disk to the star to DM ratio. As more and more baryon assemble in the central stellar disk, their luminosity increases but also the disk rotation velocity due

to the gravity of the additional matter near the center. This effect is amplified as the additional gravity also pulls dark matter towards the center. The solid-line curves in figure 7 (right) illustrate this effect for three representative dark halos of different mass (or luminosity, since a constant mass-to-light ratio of  $\Upsilon_I = 2$  is assumed). In each case the total disk mass varies from zero to  $M_{\text{disk,max}}$ , the maximum value compatible with the baryonic content of the halo, the rightmost point of each curve. As the disk mass increases, each hypothetical galaxy moves from left to right across the plot. When the disk mass becomes comparable to the dark mass inside  $2.2r_{\text{disk}}$  the curve inches upwards and becomes essentially parallel to the observed TF relation. Consequently a variation in the star to dark matter fraction results in a shift parallel to the TF relation and thus does not cause a substantial additional scatter.

It is also clear from figure 7 why the models fail to reproduce the observed zero-point of the TF relation. Even under the extreme assumption that galaxies contain *all* available baryons in each halo, simulated disks are almost two magnitudes fainter than observed. Increasing the baryonic mass of a halo has virtually no effect on this conclusion, since in this case model galaxies would just move further along paths approximately parallel to the TF relation, as shown in figure 7. Disk galaxies assembled inside CDM halos therefore cannot match the observed TF relation.

Perhaps the most uncertain step in this argument is the stellar mass-to-light ratio adopted for the analysis. The horizontal “error bar” shown on the starred symbols in figure 7 indicates the effect of varying the *I*-band mass-to-light ratio by a factor of two from the fiducial value of 2 in solar units. This is not enough to restore agreement with observations, which would require  $(M_{\text{disk}}/L_I) \sim 0.4$ , a value much too low to be consistent with standard population synthesis models. The vertical “error bars” illustrate the effect of varying the “concentration” of each halo by a factor of two. Even with this large variation in halo structure, the model disks fail to reproduce the observations.

The mismatch of the zero-point of the TF relation is closely linked to the failure to reproduce the dynamics of the Milky Way discussed earlier. Because the dark halos are quite centrally concentrated, the assembly of a massive galaxy at the center raises  $v_{\text{rot}}$  above and beyond the halo circular velocity, by up to 60%. The only way to collect a massive disk galaxy without increasing  $v_{\text{rot}}$  significantly over  $v_{\text{vir}}$  is to have dark halos that are less centrally concentrated, consistent with the conclusion of section 3.

## 6. Summary and Conclusions

I presented results on recent efforts to model the formation and evolution of galaxies in a hierarchical structure universe using high resolution computer simulations. I demonstrated that only numerical simulation can take full account of the dynamic of the formation process and the complicated interplay between different physical processes such as, e.g. , accretion and merging, star formation and feedback, photo heating and radiative cooling. Observational data can easily be misinterpreted if these effects are not properly included. For example, the apparent inconsistency of hierarchical structure models and the kinematics of high- $z$  damped Ly- $\alpha$  absorption systems could be easily solved by properly accounting for the complicated non-equilibrium dynamics of galaxies in the process of formation. Further successes include:

- Gaseous and stellar disks resembling spiral galaxies can readily be produced in numerical simulations. Merging of spiral galaxies can trigger star burst and result in the formation of ellipticals.
- Adopting star formation recipes that match observational constraints (e.g. Kennicutt’s law), the slope and scatter of the TF can be easily reproduced in such numerical simulations.

However, numerical simulations also unraveled a number of serious inconsistencies of currently favored structure formation models:

- Structure formation models such as the different flavors of the cold dark matter scenario make strong predictions on the profiles of dark matter halos. However, models such as the  $\Lambda$ CDM model predict dark matter halos that are too concentrated to be consistent with the rotation curves of disk galaxies, the kinematics of the Milky Way and the zero point of the TF relation.
- The probably most serious problem of hierarchical clustering scenarios is related to the angular momentum of disk galaxies. Tidal torques, which spin up dark matter halos early on in their formation history, only provide marginally enough angular momentum to explain the sizes of present day disk galaxies. Maintaining the hierarchical build-up of galaxies and simultaneously avoiding substantial exchange of angular momentum from the gas to the dark matter due to mergers appears to be a major challenge.

But the probably even more important result is that numerical simulations have demonstrated to be capable of making strong, falsifiable

predictions on the structure of galaxies at length scales of several kpc and smaller. The new 8m-class telescopes and proposed space missions will be able to probe this exact length scale in high- $z$  galaxies. Numerical simulations thus provide an indispensable tool for establishing the theoretical framework within which these new observations can be interpreted.

### Acknowledgements

This article includes work from collaborations with M. Haehnelt, A. Huss, B. Jain, J. Navarro and M. Rauch. This work has been supported by the National Aeronautics and Space Administration under NASA grant NAG 5-7151, by the National Science Foundation under NSF grant 9807151, and by fellowships from the Alfred P. Sloan Foundation and the David and Lucile Packard foundation. Travel support to participate the conference was provided by the Anglo American Chairman's Fund, and SASOL. I also acknowledge the hospitality of the Max-Planck Institut für Astronomie and of the Max-Planck Institut für Astrophysik, where parts of this manuscript have been written.

### References

- Abel, T., Anninos, P., Norman, M.L., Zhang, Y., 1998, ApJ, 508, 518.  
van Albada, T. S., 1982, MNRAS, 201, 939.  
Barnes, J., Efstathiou, G., 1987, ApJ, 319, 575.  
Barnes, J., Hernquist, L., 1992, ARA&A, 30, 705.  
Bartelmann, M., Steinmetz, M., 1996, MNRAS, 284, 431.  
Bartelmann, M., Steinmetz, M., Weiss, A., 1995, A&A, 297, 1.  
Cen, R., Miralda-Escudé, J., Ostriker, J.P., Rauch, M., 1994, ApJ, 437, 9.  
Cole, S.M., Aragón-Salamanca, A., Frenk, C.S., Navarro, J.F., Zepf, S.E., 1994, MNRAS, 271, 781.  
Cole, S., Lacey, C., 1996, MNRAS, 281, 716.  
Dubinski, J., Carlberg, R.G., 1991, ApJ, 378, 496.  
Evrard, A.E., Metzler, C.E., Navarro, J.F., 1996, ApJ, 469, 494.  
Ewald, P.P., 1921, Ann. Phys., 64, 253.  
Fall, S.M., 1983, in *Internal Kinematics and Dynamics of Galaxies*, Athanassoula E. (ed.), (Dordrecht: Reidel), p. 391.  
Fall, S.M., Efstathiou, G., 1980, MNRAS, 193, 189.  
Flores, R.A., Primack, J.R., 1994, ApJ, 427, L1. 317, 595.  
Giovannelli, R., Haynes, M.P., Herter, T., Vogt, N.P., 1997, AJ, 113, 22.  
Gnedin, N.Y., Ostriker, J.P., 1997, ApJ, 486, 581.  
Han, M., Mould, J.R., 1992, ApJ, 396, 453.  
Haehnelt, M., Steinmetz, M., Rauch, M., 1998, ApJ, 495, 647.  
Hernquist L., 1990, ApJ, 356, 359.

- Hernquist, L., Bouchet, F., Suto, Y., 1991, *ApJS*, 75, 231.
- Hernquist, L., Katz, N., Weinberg, D.H., Miralda–Escude J., 1996, *ApJ*, 457, L51.
- Huss A., Jain B., Steinmetz M., 1999a, *MNRAS*, in press.
- Huss A., Jain B., Steinmetz M., 1999b, *ApJ*, 517, 64.
- Kauffmann, G., 1996, *MNRAS*, 281, 475.
- Kauffmann, G., Nusser, A., Steinmetz, 1997, *MNRAS*, 286, 795.
- Kauffmann, G., White, S.D.M., Guiderdoni, B., 1994, *MNRAS*, 267, 981.
- Katz, N., 1992, *ApJ*, 391, 502.
- Katz, N., White, S.D.M., 1993, *ApJ*, 412, 455.
- Kennicutt, R.C., 1998, *ARA&A*, 36, 189.
- Klypin, A., Gottlöber, S., Kravtsov, A.V., Khokhlov, A.M., 1999, *ApJ*, 516, 530.
- Klypin, A., Kravtsov, A.V., Valenzuela, O., Prada, F., 1999, *ApJ*, 552, 82.
- Kravtsov, A.V., Klypin, A.A., Bullock, J.S., Primack, J.R., 1998, *ApJ*, 502, 48.
- Mathewson, D.S., Ford, V.L., Buchhorn, M., 1992, *ApJS*, 81, 413
- McGaugh, S.S., De Block, W.J.G. 1998, *ApJ*, 499, 41.
- Mihos, C., Hernquist, L., 1994, *ApJ*, 431, 9.
- Mo, H.J., Mao, S., White, S.D.M., 1998, *MNRAS*, 295, 319.
- Moore, B., 1994, *Nature*, 370, 629.
- Moore, B., Governato, F., Quinn, T., Stadel, J., Lake, G., 1998, *ApJ*, 499, 5.
- Moore, B., Quinn, T., Governato, F., Stadel, J., Lake, G., 1999a, *MNRAS* submitted, (astro-ph/9903164).
- Moore, B., Ghigna, S., Governato, F., Lake, G., Quinn, T., Stadel, J., 1999b, *ApJ* (Letters), in press (astro-ph/9907411).
- Navarro, J.F., 1999, *ApJ*, submitted (astro-ph 9807084).
- Navarro, J.F., Benz W., 1991, *ApJ*, 380, 320.
- Navarro, J.F., Frenk, C.S., White, S.D.M., 1995, *MNRAS*, 275, 56.
- Navarro, J.F., Frenk, C.S., White, S.D.M., 1996, *ApJ*, 462, 563.
- Navarro, J.F., Frenk, C.S., White, S.D.M., 1997, *ApJ*, 490, 493 (NFW).
- Navarro, J.F., Steinmetz, M., 1997, *ApJ*, 478, 13.
- Navarro, J.F., Steinmetz, M., 1999, *ApJ*, in press (astro-ph/9908114) (NS99).
- Navarro, J.F., White, S.D.M., 1993, *MNRAS*, 265, 271.
- Prochaska, J. X., Wolfe, A. M. 1998, *ApJ*, 507, 113.
- Rubin, V.C., Thonnard, N., Ford, V.K., 1978, *ApJ*, 225, L107.
- Steidel, C.C., Adelberger, K.L., Dickinson, M., Giavalisco, M., Pettini, M., Kellogg, M., 1998, *Astrophys. J.*, 492, 428.
- Steinmetz, M., 1996, *MNRAS*, 276, 1005.
- Steinmetz, M., Müller, E., 1994, *A&A*, 281, L97.
- Steinmetz, M., Müller, E., 1995, *MNRAS*, 276, 549.
- Steinmetz, M., Navarro, J.F., 1999, *ApJ*, 513, 555.
- Sugimoto, D., Chikada, Y., Makino, J., Ito, T., Ebisuzaki, T., Umemura, M., 1990 *Nature* **345** 33
- Syer, D., White, S.D.M., 1998, *MNRAS*, 293, 337.
- Tormen, G., Bouchet, F.R., White, S.D.M., 1997, *MNRAS*, 286, 865.
- Weil, M.L., Eke, V.R., Efstathou, G., 1998, *MNRAS*, 300, 773.
- White, S.D.M., Navarro, J.F., Evrard, A.E., & Frenk, C.S., 1993, *Nature*, 366, 429.
- Wolfe, A.M., 1988, in *QSO Absorption Lines: Probing the Universe*, Proc. of the QSO Absorption Line Meeting, Baltimore, 1987, Cambridge University Press.
- Yepes, G., Kates, R., Khokhlov, A., Klypin, A., 1997, *MNRAS*, 284, 235.
- Zhang, Y., Anninos, P., Norman, M.L., 1995, *ApJ*, 453, L57.